

# Operational Emergence of a Global Phase under Time-Dependent Coupling in Oscillator Networks

Verónica Sanz<sup>1</sup>

<sup>1</sup>*Theoretical Physics Department, Universitat de València, and  
Instituto de Física Corpuscular (IFIC), CSIC–Universitat de València, Spain*

(Dated: March 9, 2026)

Collective synchronization is often summarized by a complex order parameter  $Re^{i\Psi}$ , implicitly treating the global phase  $\Psi$  as a meaningful macroscopic coordinate. Here we ask when  $\Psi$  becomes *operationally well-defined* in oscillator networks whose coupling varies in time. We study damped (and optionally inertial) phase-oscillator models on graphs with time-dependent coupling  $K(t)$ , covering standard Kuramoto dynamics as a limit and including network and spatial topologies relevant to engineered settings.

We propose an operational emergence criterion: a macroscopic phase is emergent only when it is robustly estimable, which we quantify via gauge-fixed phase-lag fluctuations under weak noise and finite sampling. This yields a quantitative threshold controlled by  $NR^2$  and makes explicit why  $\Psi$  is ill-posed in incoherent states even when formally definable. Nonautonomous coupling introduces a ramp timescale that competes with relaxation. Using a Laplacian-mode reduction near coherence, we derive a graph-spectral rate criterion: ordering tracks the protocol when  $K(t)\lambda_2$  dominates the ramp rate, while faster ramps induce freeze-out. Numerically, we extract an operational freeze-out time from an energy-based tracking diagnostic and show that, for non-spatial networks, the residual incoherence at freeze-out collapses when plotted against the spectral protocol parameter  $\lambda_2\tau$  across Erdős–Rényi and small-world graph families. Finally, on periodic lattices we show that topological sectors and defect-mediated ordering obstruct complete alignment, leading to protocol-dependent, long-lived partially synchronized states and systematic deviations from spectral collapse.

## I. INTRODUCTION

Synchronization theory provides a compact language for collective dynamics across physical, biological, and engineered systems. A canonical reduction is the complex order parameter

$$Z(t) \equiv R(t)e^{i\Psi(t)} := \frac{1}{N} \sum_{j=1}^N e^{i\theta_j(t)}, \quad (1)$$

where  $R \in [0, 1]$  measures coherence and  $\Psi$  is often interpreted as a global reference phase. Yet this interpretation hides an operational subtlety: when  $R \simeq 0$ , the phase of  $Z$  is effectively undefined, and finite sampling or weak noise can induce order-one excursions of  $\Psi$ . The question we address is therefore not merely definitional but physical: *when does a macroscopic reference phase exist as a robust, usable coordinate?*

We focus on *nonautonomous* synchronization, where the effective coupling varies in time. Time dependence is ubiquitous in practice: interaction strengths are modulated by external drives, resources and links can be intermittently available, and control parameters are routinely scheduled. In such settings, ordering is governed by a competition between (i) intrinsic relaxation of phase differences on the graph and (ii) the external ramp timescale. Our main message is that this competition controls a sharp form of *rate-dependent emergence*: slow protocols allow coherence (and hence a usable reference phase) to develop and persist, whereas fast ramps can suppress ordering even when the instantaneous coupling becomes large.

This work is motivated in part by a cosmology-driven perspective. In [1] we pointed out that axion misalignment can be viewed through the lens of synchronization: a large population of oscillating degrees of freedom can develop collective phase structure whose observational imprint depends on how “coordination” emerges. Here we abstract that viewpoint into a general theoretical framework for nonautonomous oscillator networks, with the aim of exporting the core mechanisms to broader synchronization settings where emergence and timescale competition are central.

*What we show (and how we test it).* Our results sharpen three statements that are borne out by explicit simulations. First, the global phase  $\Psi$  becomes operational only once coherence is sufficiently large: we quantify phase robustness via lagged, gauge-fixed phase fluctuations and show that phase uncertainty is strongly suppressed as a function of  $NR^2$ . Second, protocol dependence is organized by graph relaxation scales: for generic networks we find that residual incoherence at the operational freeze-out time collapses when plotted against the spectral protocol parameter  $\lambda_2\tau$  (with  $\lambda_2$  the Laplacian gap and  $\tau$  a ramp timescale), supporting a graph-spectral rate criterion for adiabatic tracking versus freeze-out. Third, periodic spatial graphs can evade this collapse: rings (and, by extension, lattices with periodic

boundary conditions) systematically deviate because topological sectors and defect-mediated coarsening obstruct full ordering, yielding persistent partially synchronized states whose statistics depend on the protocol.

*Contributions.* (i) We introduce an *operational emergence criterion* for the global phase based on robustness/estimability, implemented via phase-lag statistics and a coherence-controlled threshold that scales with  $NR^2$ . (ii) We derive and validate a *graph-spectral rate criterion* in terms of the algebraic connectivity  $\lambda_2$ , and show that protocol dependence across non-spatial graphs is organized by  $\lambda_2\tau$ . (iii) We identify *topological obstruction* as a distinct mechanism on periodic spatial graphs, leading to systematic deviations from network collapse and to protocol-dependent long-lived partial ordering.

## II. RELATED WORK

The Kuramoto model and its extensions provide a canonical framework for collective synchronization, including mean-field theory, bifurcation structure, and broad connections to physical, biological, and engineered systems. A comprehensive reference is the review by Acebrón *et al.* [2]. Network generalizations and their implications for synchronization thresholds and stability are reviewed in Dörfler and Bullo [3], while the onset of synchronization in heterogeneous networks can be controlled by spectral properties (e.g. adjacency eigenvalues), as shown by Restrepo, Hunt, and Ott [4]. Time dependence is a natural ingredient in thermodynamically open or externally driven settings: Petkoski and Stefanovska studied Kuramoto dynamics with explicitly time-varying parameters and clarified non-adiabatic responses to external modulation [5]. A complementary line of work establishes the robustness of low-dimensional reductions: Pietras and Daffertshofer proved attractiveness of the Ott–Antonsen manifold in parameter-dependent oscillator networks and extended the analysis to time-dependent parameters and beyond global coupling [6]; more generally, the Ott–Antonsen reduction provides a standard backbone for macroscopic descriptions in large oscillator populations [7]. Nonautonomy can also enter through additional dynamical memory, most prominently via time delays in coupling. Early studies established that delay reshapes synchronization thresholds and can induce multistability even in globally coupled populations [8], with detailed analyses for structured frequency distributions such as bimodal cases [9]. Recent work further explores delay in network settings, including attractive/repulsive delayed couplings [10] and small-world/random architectures [11], and develops bifurcation-based descriptions in the time-delayed Kuramoto model [12]; very recent studies examine the interplay of delay and inertia in second-order networks, highlighting delay-induced multistability among phase-locked states [13]. Beyond delays, a substantial literature addresses synchronization on *time-varying networks* (edge rewiring or switching topologies), where nonautonomy enters through  $A_{ij}(t)$ . For example, Faggian *et al.* studied synchronization in time-varying random networks and provided analytical arguments based on competing timescales (rewiring vs. intrinsic relaxation), identifying regimes where partial synchronization can emerge even at vanishing connectivity in appropriate limits [14]. In multiplex settings, time-switching of interlayer connections can induce abrupt transitions in interlayer synchrony and reshape basins of attraction [15]. From a control/consensus perspective, stability under time-varying topologies and time delays has been studied under broad stochastic switching assumptions [16], and time variation can also be treated as a design knob: Leander *et al.* found that time-varying connectivity can be more efficient than static architectures at promoting synchrony in controlled Kuramoto networks [17].

A parallel strand concerns *quenches*, freeze-out, and defect-mediated ordering in spatially extended synchronization. Miranda *et al.* reported defect trapping and “frozen” dynamics in synchronization fronts with an explicit Kibble–Zurek interpretation [18]. For the short-range noisy Kuramoto model in two dimensions, Rouzairé and Levis analyzed defect dynamics following a quench, including inertial vs overdamped comparisons and the role of vortices in the ordering process [19]. Defect-centric viewpoints have also been advanced for the entrainment transition in the two-dimensional Kuramoto model, where vortex dynamics delineate coherent clusters [20], and for periodic lattices via vortices and duality-based descriptions [21]. Finite-size effects shape both the approach to the thermodynamic limit and the fluctuations of the macroscopic order parameter: Coletta, Delabays, and Jacquod studied finite-size scaling near the locking threshold and clarified convergence to infinite- $N$  behavior [22] (see also Pazó [23] for critical scaling in the thermodynamic limit). Recently, Omel’chenko and Gottwald developed an ab initio mean-field approach for finite-size fluctuations in the Kuramoto–Sakaguchi model, obtaining explicit covariance expressions for order-parameter fluctuations [24]. In parallel, information-theoretic lenses have been applied to synchronization criticality, e.g. via Fisher information [25]. Finally, a growing literature on *rate-induced tipping* (R-tipping) emphasizes that rapid parameter change can induce qualitative transitions even without crossing a classical bifurcation; although much of this work is developed in broader dynamical-systems contexts (including oscillatory ecological models and multistable oscillator systems) [26, 27], its core mechanism aligns naturally with nonautonomous synchronization when the system cannot track a moving quasi-steady state.

Building on these strands, we focus on *nonautonomous emergence* of a *reference phase* in a deliberately minimal setting: a fixed graph with a time-dependent coupling protocol  $K(t)$ . Our first contribution is to make the exis-

tence of a global phase  $\Psi$  *operational* by tying it to robustness/estimability under finite- $N$  fluctuations and weak noise, thereby distinguishing regimes where  $\Psi$  is well-defined from regimes where it is ill-posed. Second, we connect rate-dependent ordering under  $K(t)$  to graph relaxation timescales and explicitly expose the role of graph spectrum (notably the algebraic connectivity  $\lambda_2$ ) in adiabatic tracking versus freeze-out, complementing spectral threshold results for autonomous networks [3, 4]. Third, on periodic spatial graphs we unify protocol dependence with topological obstruction by quantifying how ramps shape defect/topological-charge statistics and long-lived partially synchronized states, linking quench/defect and vortex-based pictures [18–21] to a graph-based nonautonomous framework. Although the present work is theoretical, our model class overlaps with power-grid-motivated Kuramoto-like reductions: Filatrella *et al.* give a classic mapping between Kuramoto-type models and power distribution grids [28], and network synchronization surveys discuss relevance to engineered oscillator networks [3]. We treat these connections as motivation; application-specific validation is deferred to future work.

### III. MODEL CLASS AND LIMITS

We consider  $N$  phase variables  $\theta_i(t) \in \mathbb{S}^1$  located on the nodes of a (possibly weighted) graph  $G = (V, E)$  with adjacency matrix  $\mathbf{A} = (A_{ij})_{i,j=1}^N$ . Unless stated otherwise we assume  $A_{ij} \geq 0$ ,  $A_{ii} = 0$ , and (for simplicity) an undirected graph  $A_{ij} = A_{ji}$ . The degree of node  $i$  is  $k_i = \sum_j A_{ij}$ . We write the complex Kuramoto order parameter

$$Z(t) \equiv R(t) e^{i\Psi(t)} := \frac{1}{N} \sum_{j=1}^N e^{i\theta_j(t)}, \quad (2)$$

and emphasize that while  $Z$  is always well-defined, the interpretation of  $\Psi$  as a macroscopic coordinate depends on the level of coherence and fluctuations (made precise in Sec. IV).

#### A. Nonautonomous inertial phase model on a graph

We study a broad class of nonautonomous phase-oscillator networks capturing inertia, damping, quenched heterogeneity, external pinning, and stochastic forcing:

$$m \ddot{\theta}_i + \gamma \dot{\theta}_i = \omega_i + K(t) \sum_{j=1}^N A_{ij} \sin(\theta_j - \theta_i) - \eta(t) \sin(\theta_i - \phi(t)) + \sqrt{2D} \xi_i(t), \quad i = 1, \dots, N. \quad (3)$$

Here  $m \geq 0$  is an inertial parameter,  $\gamma > 0$  is linear damping, and  $\omega_i$  are intrinsic frequencies (typically drawn from a distribution  $g(\omega)$ , though we will focus on the identical case  $\omega_i = 0$  for the core emergence mechanism). The coupling strength  $K(t)$  is a prescribed (deterministic) function of time; we refer to it as the *coupling protocol*. The optional pinning term of strength  $\eta(t) \geq 0$  aligns phases to an externally imposed reference phase  $\phi(t)$  (e.g. entrainment or synchronization to a global clock); it will be set to  $\eta \equiv 0$  unless stated otherwise. Finally,  $\xi_i(t)$  are independent standard Gaussian white noises,

$$\langle \xi_i(t) \rangle = 0, \quad \langle \xi_i(t) \xi_j(t') \rangle = \delta_{ij} \delta(t - t'), \quad (4)$$

and  $D \geq 0$  controls the noise strength.

See Fig. 1 for a schematic of the interaction structure and the coupling protocol.

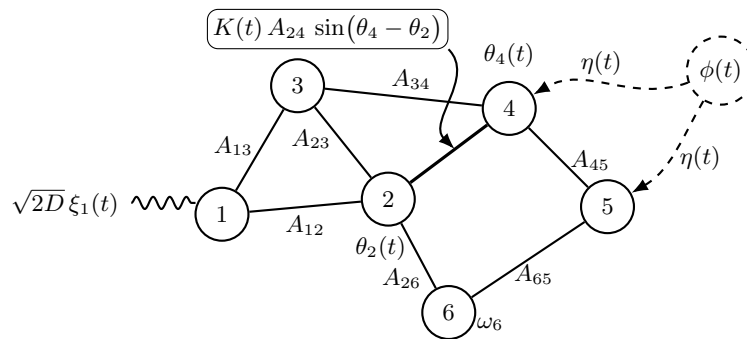
*Dimensional considerations.* With  $\theta$  dimensionless,  $K$  and  $\omega$  have units of inverse time, while  $m$  has units of time and  $\gamma$  is dimensionless in the standard nondimensionalization (or, equivalently,  $\gamma$  has units such that  $m\ddot{\theta}$  and  $\gamma\dot{\theta}$  match). A convenient rescaling of time can set  $\gamma = 1$  when  $m > 0$ , but we keep explicit parameters to facilitate comparison with inertial/swing-equation conventions.

*Protocol class.* While our theory applies to general  $K(t)$ , we will use representative monotone protocols in numerics, e.g.

$$K_{\downarrow}(t) = K_0 \left(1 + \frac{t}{\tau}\right)^{-\alpha}, \quad (5)$$

$$K_{\uparrow}(t) = K_0 \tanh\left(\frac{t}{\tau}\right), \quad (6)$$

characterized by a ramp time  $\tau$  and a shape parameter (e.g.  $\alpha$ ). These forms are chosen because the ramp rate  $\partial_t \ln K$  is explicit and supports a sharp adiabaticity criterion in terms of graph relaxation (Sec. V).



$$\text{Edges: } K(t)A_{ij} \sin(\theta_j - \theta_i) \quad \text{Pinning: } -\eta(t) \sin(\theta_i - \phi(t)).$$

FIG. 1: Schematic of the nonautonomous phase-oscillator network (3). Nodes carry phases  $\theta_i(t)$  and couple along edges with weights  $A_{ij}$  under a time-dependent protocol  $K(t)$ . A dashed reference node represents optional entrainment to  $\phi(t)$  with strength  $\eta(t)$ .

### B. Overdamped (first-order) limit

For  $m = 0$ , or more generally on timescales slow compared to the inertial relaxation time  $m/\gamma$ , Eq. (3) reduces to the first-order (overdamped) nonautonomous Kuramoto model on a graph,

$$\dot{\theta}_i = \omega_i + K(t) \sum_{j=1}^N A_{ij} \sin(\theta_j - \theta_i) - \eta(t) \sin(\theta_i - \phi(t)) + \sqrt{2D} \xi_i(t). \quad (7)$$

Unless explicitly stated, our analytical derivations of tracking versus freeze-out and the role of graph spectrum are carried out in this overdamped regime, where the slowest relaxation mode is set by the Laplacian spectral gap. We then verify numerically that the resulting scaling picture persists for moderate inertia  $m > 0$ .

### C. Graph Laplacian and linearized relaxation

Let  $\mathbf{D}$  be the degree matrix,  $D_{ii} = k_i = \sum_j A_{ij}$ , and define the (combinatorial) graph Laplacian

$$\mathbf{L} := \mathbf{D} - \mathbf{A}. \quad (8)$$

For undirected graphs  $\mathbf{L}$  is symmetric positive semidefinite with eigenvalues  $0 = \lambda_1 < \lambda_2 \leq \dots \leq \lambda_N$ . Near a coherent state in which phase differences are small,  $\sin(\theta_j - \theta_i) \approx (\theta_j - \theta_i)$  and the coupling term becomes  $-\sum_j L_{ij}\theta_j$ . In vector form, the overdamped dynamics (7) linearize to

$$\dot{\boldsymbol{\theta}} \approx \boldsymbol{\omega} - K(t) \mathbf{L} \boldsymbol{\theta} - \eta(t) (\boldsymbol{\theta} - \phi(t) \mathbf{1}) + \sqrt{2D} \boldsymbol{\xi}(t), \quad (9)$$

where  $\mathbf{1}$  is the all-ones vector. Decomposing  $\boldsymbol{\theta}$  into Laplacian eigenmodes,  $\boldsymbol{\theta}(t) = \sum_{\alpha} c_{\alpha}(t) \mathbf{v}^{(\alpha)}$ , yields for  $\alpha \geq 2$

$$\dot{c}_{\alpha}(t) \approx -K(t) \lambda_{\alpha} c_{\alpha}(t) \quad (\eta = 0, \omega_i = 0, D = 0), \quad (10)$$

so the slowest relaxation rate is controlled by the algebraic connectivity  $\lambda_2$ . This observation underpins our graph-spectral adiabaticity criterion: the system tracks a slowly varying coupling protocol when  $K(t)\lambda_2$  dominates the protocol ramp rate  $|\partial_t \ln K(t)|$  (Sec. V).

### D. Limits, connections, and interpretive remarks

Equation (3) unifies several widely used synchronization models:

1. *Standard Kuramoto*. Setting  $m = 0$ ,  $\eta = 0$ ,  $D = 0$ , and  $K(t) \equiv K$  constant gives the classical Kuramoto model on a graph.

2. *Inertial Kuramoto / swing equation.* For  $m > 0$  and  $\gamma > 0$  with graph coupling, Eq. (3) matches the standard second-order (rotor) Kuramoto form used in power-grid reductions and other oscillator networks, with  $m$  interpreted as inertia and  $\gamma$  as damping.
3. *Relaxational phase-ordering on lattices.* For identical oscillators ( $\omega_i = 0$ ) with local coupling and  $m = 0$ , Eq. (7) becomes a short-range phase-ordering dynamics (an  $XY$ /compact-phase analogue) in which defects/topological sectors can obstruct complete ordering on periodic domains.
4. *Pinned/entrained oscillators.* For  $\eta(t) \neq 0$  and prescribed  $\phi(t)$ , the model describes entrainment to an external reference; in the static case  $\phi = \text{const}$  this is equivalent to a periodic pinning potential.

*Scope of analysis.* Our main theoretical focus is the emergence of a macroscopic reference phase under nonautonomous coupling protocols on a fixed graph. Accordingly, we emphasize the identical-oscillator case  $\omega_i = 0$  and  $\eta = 0$  to isolate the emergence mechanism, and we treat weak noise  $D > 0$  as a controlled probe of robustness and estimability. Heterogeneous frequencies, explicit pinning, time delays, and time-varying topologies are natural extensions and will be discussed as outlook (Sec. VIII).

#### IV. OPERATIONAL EMERGENCE OF THE GLOBAL PHASE

The complex order parameter

$$Z(t) \equiv R(t)e^{i\Psi(t)} = \frac{1}{N} \sum_{j=1}^N e^{i\theta_j(t)} \quad (11)$$

always defines a *formal* phase  $\Psi$  whenever  $Z \neq 0$ . However, the interpretation of  $\Psi$  as a macroscopic coordinate—a “reference phase” shared by the population—is *operational*: it is meaningful only insofar as it is robust to finite-size fluctuations, weak noise, and finite-time estimation. In particular, when  $R \approx 0$  the mapping from the microscopic state  $\{\theta_i\}$  to  $\Psi$  becomes ill-conditioned: arbitrarily small perturbations of  $\{\theta_i\}$  can produce  $O(1)$  changes in  $\Psi$ . This section makes this notion quantitative by turning robustness into an emergence condition.

##### A. Robustness and estimability of $\Psi$

We use weak stochastic forcing as a controlled probe of robustness. Consider the dynamics (3) (or its overdamped limit (7)) with  $D > 0$  small. Writing  $Z = X + iY$  with  $X = \frac{1}{N} \sum_j \cos \theta_j$  and  $Y = \frac{1}{N} \sum_j \sin \theta_j$ , we have

$$\Psi = \arg Z = \arctan\left(\frac{Y}{X}\right), \quad R = \sqrt{X^2 + Y^2}. \quad (12)$$

In the coherent regime ( $R$  not too small) the fluctuations of  $X$  and  $Y$  induced by noise and finite  $N$  are typically  $O(N^{-1/2})$ . Propagating these fluctuations to  $\Psi$  yields the generic scaling

$$\text{Var}(\Psi) \sim \frac{D_{\text{eff}}}{N R^2}, \quad (13)$$

where  $D_{\text{eff}}$  is an effective noise level that absorbs model-dependent prefactors, correlations, and finite-time sampling effects.<sup>1</sup> Equation (13) makes explicit a key point: the uncertainty of the global phase diverges as  $R \rightarrow 0$  even at fixed  $N$ , and decreases only when coherence and/or population size are sufficiently large.

*Operational emergence threshold.* We say that the global phase  $\Psi$  is *emergent* when it can be estimated with small uncertainty on the timescales of interest. Concretely, fix a tolerance  $\sigma_\Psi^2 \ll 1$  (e.g.  $\sigma_\Psi \sim 0.1$  rad) and declare  $\Psi$  emergent when  $\text{Var}(\Psi) \leq \sigma_\Psi^2$ . Using (13), this is equivalent to a threshold on the “phase signal-to-noise”

$$N R^2 \gtrsim \kappa, \quad \kappa := \frac{D_{\text{eff}}}{\sigma_\Psi^2} = O(1-10) \text{ in typical dimensionless units,} \quad (14)$$

where the precise numerical value depends on the measurement protocol and the effective noise level. The condition (14) captures the system-size dependence of emergence: for fixed coherence  $R$ , larger populations yield a sharper (more robust) reference phase, while for fixed  $N$  the reference phase becomes well-defined only after the system has dynamically generated sufficient coherence.

<sup>1</sup> The  $1/(NR^2)$  dependence reflects the fact that phase fluctuations are amplified when the order-parameter magnitude is small. This scaling is consistent with standard error-propagation arguments for  $\Psi = \arg Z$  and with finite-size fluctuation theories for the order parameter. In Sec. VII we verify the scaling empirically and treat  $D_{\text{eff}}$  as a fitted quantity when needed.

*Emergence time under nonautonomous protocols.* For a time-dependent coupling protocol  $K(t)$ , the condition (14) defines an *emergence time*  $t_{\text{em}}$  as the first time at which  $NR(t)^2$  crosses  $\kappa$  (optionally with a persistence requirement over a time window). This provides a practical diagnostic to compare protocols and graph families: emergence is not merely “large  $R$ ”, but the moment when the macroscopic phase becomes a stable, reproducible coordinate.

### B. Estimating $\text{Var}(\Psi)$ in simulations

In numerical experiments we estimate  $\text{Var}(\Psi)$  in three complementary ways:

1. *Ensemble variance:* run  $M$  realizations with independent noise and/or random initial conditions at fixed parameters and compute the sample variance of  $\Psi(t)$  across realizations.
2. *Time-window variance:* in stationary or quasi-stationary regimes, compute the variance of  $\Psi(t)$  over a sliding window  $[t, t + \Delta t]$  (after unwrapping  $\Psi$  to avoid  $2\pi$  discontinuities).
3. *Controlled perturbations:* apply small random phase kicks  $\theta_i \rightarrow \theta_i + \delta\theta_i$  with  $\delta\theta_i$  i.i.d. of variance  $\sigma_\theta^2$  and measure the induced dispersion of  $\Psi$ .

All three procedures quantify robustness; when the dynamics is mixing and the sampling window is long enough, the time-window and ensemble estimators agree up to finite-sample corrections.

Throughout, we report  $R(t)$  and  $\Psi(t)$  together with  $\text{Var}(\Psi(t))$  (or equivalently  $NR(t)^2$ ) as functions of protocol parameters, graph family, and system size. The pair  $(R(t), \text{Var}(\Psi(t)))$  makes explicit the distinction between *formal* existence of a phase (whenever  $Z \neq 0$ ) and *operational* emergence of a macroscopic reference phase.

## V. RATE-CONTROLLED EMERGENCE UNDER TIME-DEPENDENT COUPLING

We now quantify how a nonautonomous coupling protocol  $K(t)$  controls ordering and, consequently, the operational emergence of a macroscopic reference phase. The key point is that ordering on a graph is not instantaneous: phase differences relax on timescales set by the graph Laplacian spectrum. A time-dependent protocol introduces an external timescale (the ramp), and the competition between the two determines whether the system can track the “instantaneous” ordering tendency or instead falls out of quasi-equilibrium (freeze-out).

Throughout this section we focus on the overdamped, identical-oscillator case ( $m = 0$ ,  $\omega_i = 0$ ) with no pinning ( $\eta = 0$ ), as it isolates the emergence mechanism and yields transparent spectral criteria. Extensions to inertia and weak disorder are addressed numerically in Sec. VII.

### A. Spectral mode reduction and relaxation rates

Consider the overdamped dynamics (7) with  $D = 0$  and small phase differences, so that  $\sin(\theta_j - \theta_i) \approx \theta_j - \theta_i$ . In vector form,

$$\dot{\boldsymbol{\theta}} \approx -K(t) \mathbf{L} \boldsymbol{\theta}, \quad (15)$$

where  $\mathbf{L}$  is the graph Laplacian (8). Let  $\{\mathbf{v}^{(\alpha)}\}$  be Laplacian eigenvectors,  $\mathbf{L}\mathbf{v}^{(\alpha)} = \lambda_\alpha \mathbf{v}^{(\alpha)}$  with  $0 = \lambda_1 < \lambda_2 \leq \dots \leq \lambda_N$ . Expanding  $\boldsymbol{\theta}(t) = \sum_\alpha c_\alpha(t) \mathbf{v}^{(\alpha)}$  yields, for all nontrivial modes  $\alpha \geq 2$ ,

$$\dot{c}_\alpha(t) \approx -K(t) \lambda_\alpha c_\alpha(t). \quad (16)$$

Thus each mode decays with an instantaneous rate  $K(t)\lambda_\alpha$  and the slowest relaxation is controlled by the spectral gap  $\lambda_2$  (algebraic connectivity). This immediately identifies the intrinsic graph-controlled relaxation timescale

$$\tau_{\text{rel}}(t) \sim \frac{1}{K(t)\lambda_2}. \quad (17)$$

While the linearization is formally valid near coherence, it provides the correct scaling variable that organizes the nonlinear numerics: protocol dependence enters primarily through how  $K(t)$  compares to the slowest graph relaxation.

## B. Adiabatic tracking versus freeze-out

To quantify the protocol timescale, define the instantaneous ramp time as

$$\tau_{\text{ramp}}(t) \sim \left| \frac{d}{dt} \ln K(t) \right|^{-1}. \quad (18)$$

If  $\tau_{\text{rel}} \ll \tau_{\text{ramp}}$ , relaxation is fast compared to protocol change and the system can track the ordering tendency associated with the instantaneous coupling; if  $\tau_{\text{rel}} \gg \tau_{\text{ramp}}$ , the protocol changes faster than the graph can relax and the state falls out of quasi-equilibrium.

This motivates the adiabatic tracking condition

$$K(t)\lambda_2 \gg \left| \frac{d}{dt} \ln K(t) \right|. \quad (19)$$

When (19) fails, coherence no longer follows the slowly varying quasi-steady ordering manifold. We define a characteristic *freeze-out time*  $t_*$  by the implicit balance

$$K(t_*)\lambda_2 \sim \left| \frac{d}{dt} \ln K(t) \right|_{t=t_*}. \quad (20)$$

Intuitively,  $t_*$  marks the last time at which the slowest collective mode can still equilibrate to the protocol. Beyond  $t_*$  (for a decreasing protocol) the system retains a memory of the coherence it has built up, and the final coherence  $R_\infty$  is controlled by the state at freeze-out up to subsequent slow coarsening and defect dynamics on spatial graphs.

*Connection to operational emergence.* Combining Sec. IV with (20), the protocol also controls the *emergence time*  $t_{\text{em}}$  defined by the threshold  $NR(t_{\text{em}})^2 \gtrsim \kappa$ . In practice,  $t_{\text{em}}$  is bounded by the same competition: if coherence cannot build up fast enough before freeze-out, the reference phase may never become operationally well-defined on the timescale of the protocol.

## C. Representative protocols and explicit $t_*$ estimates

We will consider monotone protocols as canonical test cases:

$$K_\downarrow(t) = K_0 \left( 1 + \frac{t}{\tau} \right)^{-\alpha}, \quad (21)$$

$$K_\uparrow(t) = K_0 \tanh\left(\frac{t}{\tau}\right), \quad (22)$$

and, where useful, pulsed variants. The decay protocol (21) is analytically convenient since

$$\frac{d}{dt} \ln K_\downarrow(t) = -\frac{\alpha}{t + \tau}. \quad (23)$$

Substituting into (20) gives an explicit implicit equation for  $t_*$ :

$$K_0 \left( 1 + \frac{t_*}{\tau} \right)^{-\alpha} \lambda_2 \sim \frac{\alpha}{t_* + \tau}. \quad (24)$$

For increasing protocols such as (22),  $t_*$  instead characterizes the crossover from non-adiabatic growth of coherence to adiabatic tracking as  $K(t)$  becomes large enough; Eq. (20) still defines the crossover scale.

## D. Scaling variables and testable collapse

Equation (20) shows that protocol dependence enters through combinations of the ramp parameters with the graph spectral gap  $\lambda_2$ . This motivates using  $\lambda_2$  as the primary graph descriptor for comparing different topologies at fixed  $N$ . For the protocol families (21)–(22), the natural dimensionless control parameters are constructed from  $\lambda_2\tau$  and

the protocol-shape parameters (e.g.  $\alpha$ ), with additional dependence on  $N$  and noise  $D$  through finite-size fluctuations and defect dynamics.

Accordingly, we will test scaling collapses of the form

$$R_\infty = \mathcal{F}(\lambda_2 \tau; \alpha, D, N), \quad (25)$$

and similarly for (i) the emergence time  $t_{\text{em}}$  defined by  $NR(t_{\text{em}})^2 \simeq \kappa$ , and (ii) the robustness metric  $\text{Var}(\Psi)$ . In spatial graphs where coarsening and defects dominate long-time behavior,  $R_\infty$  may be replaced by a protocol-dependent correlation length or defect density, but the organizing role of  $\lambda_2$  and the ramp rate remains the same.

## VI. TOPOLOGICAL OBSTRUCTION AND DEFECT SECTORS ON PERIODIC GRAPHS

When the coupling graph admits a spatial embedding with periodic boundary conditions—most notably rings ( $\mathbb{S}^1$ ) and two-dimensional tori ( $\mathbb{T}^2$ )—the phase field  $\theta$  supports topological sectors. These sectors are invisible in purely mean-field descriptions but can dominate long-time dynamics under local coupling: even when interactions favor alignment, the system may be unable to reach the fully synchronized state without rare phase-slip events. In the present context this provides a second, independent obstruction to the emergence of a global reference phase: a system may develop substantial local coherence while remaining globally frustrated by nontrivial topological charge.

### A. Winding sectors on a ring

Consider a ring graph with nearest-neighbor coupling and periodic indexing  $\theta_{N+1} \equiv \theta_1$ . Define the wrapped phase increment on each edge by

$$\Delta_i := \text{wrap}(\theta_{i+1} - \theta_i) \in (-\pi, \pi], \quad (26)$$

and the (integer-valued) winding number

$$W := \frac{1}{2\pi} \sum_{i=1}^N \Delta_i \in \mathbb{Z}. \quad (27)$$

The integer  $W$  labels homotopy sectors of maps  $\theta : \mathbb{S}^1 \rightarrow \mathbb{S}^1$  and provides a convenient coarse-grained descriptor of global frustration:  $W = 0$  corresponds to an untwisted sector compatible with complete alignment, while  $W \neq 0$  implies that the phase winds by  $2\pi W$  around the ring and perfect synchronization (all  $\theta_i$  equal) is topologically forbidden.

In the noiseless overdamped dynamics with smooth evolution,  $W$  is conserved: changing  $W$  requires a *phase slip* in which at least one increment  $\theta_{i+1} - \theta_i$  crosses the branch cut at  $\pm\pi$ , corresponding to a local “defect” event. For finite  $N$  and nonzero noise  $D$ , phase slips occur with a rate that depends strongly on the effective coupling scale, so  $W$  can become metastable on accessible timescales. As a consequence, long-lived partially synchronized states with  $R < 1$  arise naturally in sectors with  $W \neq 0$  even when local phase differences are small.

### B. Defects and vortices on higher-dimensional periodic lattices

On a two-dimensional periodic lattice, the analogous topological excitations are vortices: around a closed plaquette one can define the discrete circulation  $\sum \text{wrap}(\Delta\theta)$ , whose nonzero integer values indicate vortices/antivortices. Defect-mediated ordering then proceeds via vortex annihilation and coarsening, and complete global coherence can be delayed or obstructed by long-lived defect configurations. While we will focus primarily on the ring (where the winding number provides an unambiguous integer label), the numerical diagnostics in Sec. VII extend directly to vortex densities on  $\mathbb{T}^2$ .

### C. Protocol dependence of sector statistics and residual coherence

Time-dependent coupling introduces a natural competition: defect annihilation and phase-slip dynamics require time to relax, while the protocol changes the effective barrier for defect motion and annihilation. For decreasing

protocols  $K(t)$ , the system may “freeze” into a nontrivial sector before defects can fully annihilate; for increasing protocols, defects may annihilate efficiently once  $K(t)$  becomes large enough, but the crossover depends on ramp rate. In the presence of weak noise, the protocol also controls the probability of phase slips that change the sector.

Accordingly, on rings we characterize the protocol dependence through the winding-number distribution

$$P(W) \equiv \Pr[W(t \rightarrow \infty) = W], \quad (28)$$

and the conditional residual coherence  $R_\infty(W)$ , i.e. the long-time order parameter magnitude within a given sector. On higher-dimensional periodic lattices we replace  $W$  by defect observables such as the vortex density  $\rho_v$ . In Sec. VII we quantify how  $P(W)$  (or  $\rho_v$ ) and the resulting  $R_\infty$  depend on protocol parameters (e.g.  $\tau, \alpha$  for (21)–(22)), system size  $N$ , and noise strength  $D$ . This provides a concrete link between nonautonomous protocols and topological obstruction: the protocol does not only control how fast coherence grows, but also which topological sector the system becomes trapped in, and therefore whether a robust global reference phase can emerge.

## VII. NUMERICAL EXPERIMENTS

This section validates three intertwined claims developed in Secs. IV–V: (i) time-dependent coupling protocols generate (or suppress) coherence in a rate-controlled manner, (ii) the global phase becomes *operationally* meaningful only once coherence is sufficiently large, and (iii) across non-spatial graphs, protocol dependence is organized by the spectral parameter  $\lambda_2\tau$ , while periodic spatial graphs can deviate due to topological obstruction. All simulations use the overdamped model (7) on weighted graphs with symmetric adjacency  $A$  and time-dependent coupling  $K(t)$ .

*a. Dynamics, discretization, and protocol.* We integrate the stochastic differential equation

$$\dot{\theta}_i(t) = K(t) \sum_{j=1}^N A_{ij} \sin(\theta_j - \theta_i) + \sqrt{2D} \xi_i(t), \quad \langle \xi_i(t) \xi_j(t') \rangle = \delta_{ij} \delta(t - t'), \quad (29)$$

with  $\omega_i = 0$  and no external pinning ( $\eta = 0$ ) in order to isolate protocol-driven ordering. We use Euler–Maruyama time stepping with  $\Delta t = 10^{-2}$  up to a final time  $T = 35$ . Initial phases are i.i.d. uniform on  $(-\pi, \pi]$ . Noise is weak ( $D = 10^{-3}$ ) and serves two roles: (a) to probe robustness of the global phase, and (b) to regularize ensemble statistics. The nonautonomous protocol is taken as a monotone power-law decay

$$K(t) = K_0 \left(1 + \frac{t}{\tau}\right)^{-\alpha}, \quad K_0 = 3.0, \quad \alpha = 2.0, \quad (30)$$

and we scan the ramp time  $\tau \in \{0.5, 1, 2, 4, 8\}$  for the main diagnostic plots. To accelerate simulations we implement coupling evaluation in  $O(E)$  per time step using an edge list, where  $E$  is the number of edges (rather than forming all pairwise phase differences). Each parameter point is estimated from an ensemble of  $M = 25$  independent realizations (random initial conditions and independent noise).

*b. Graph families and spectral gap.* We focus on three representative graph families:

1. Erdős–Rényi (ER) graphs  $G(N, p)$  with  $N = 80$  and  $p \in \{0.04, 0.06, 0.08\}$ , generated with connectivity enforced.
2. Watts–Strogatz (WS) small-world graphs with  $N = 80$ ,  $k = 6$ , and rewiring probability  $\beta = 0.2$  (connectivity enforced).
3. A periodic ring graph (nearest-neighbor coupling) as a canonical spatial/periodic topology where winding sectors exist.

For each graph we compute the Laplacian spectral gap  $\lambda_2$  (algebraic connectivity), which sets the slowest linear relaxation scale and enters the protocol adiabaticity criterion.

*c. Simulation parameters.* For reproducibility, the numerical setup (integration scheme, protocol parameters, graph families, and ensemble sizes) is summarized in Table I. Table II provides a comparison among the families considered in the experiments.

### Observables

*d. Order parameter and global phase.* We compute the complex order parameter

$$Z(t) = R(t) e^{i\Psi(t)} = \frac{1}{N} \sum_{j=1}^N e^{i\theta_j(t)}, \quad (31)$$

TABLE I: **Numerical setup and parameters.** Baseline simulation and analysis settings used to generate all figures in Sec. VII. Graph-specific parameters are listed separately.

Quantity	Value / definition
Model	Overdamped stochastic Kuramoto on a graph, Eq. (7)
Integrator	Euler–Maruyama
Time step	$\Delta t = 10^{-2}$
Final time	$T = 35$
Initial phases	$\theta_i(0) \sim \text{Unif}(-\pi, \pi]$ i.i.d.
Noise strength	$D = 10^{-3}$
Frequencies / pinning	$\omega_i = 0$ (identical), no pinning ( $\eta = 0$ )
Protocol	$K(t) = K_0 (1 + t/\tau)^{-\alpha}$
Protocol parameters	$K_0 = 3.0, \alpha = 2.0$
Ramp times (diagnostics)	$\tau \in \{0.5, 1, 2, 4, 8\}$
Ramp times (collapse plot)	$\tau \in \{0.5, 1.5, 4, 10\}$
System size	$N = 80$
Order parameter	$Z(t) = \frac{1}{N} \sum_j e^{i\theta_j(t)} \equiv R(t)e^{i\Psi(t)}$
Phase robustness anchor	$t_0 = 12$ for $V_\Psi(\Delta t)$
Tracking ratio	$r_E(t) = [-\frac{1}{2} \partial_t \ln E(t)] / [K(t)\lambda_2]$
Disagreement energy	$E(t) = \ \boldsymbol{\theta}(t) - \bar{\boldsymbol{\theta}}(t)\mathbf{1}\ ^2$
Freeze-out (measured)	hysteresis on $r_E(t)$ : $r_{\text{high}} = 0.7, r_{\text{low}} = 0.4$
Freeze-out windows	$t_{\text{ignore}} = 0.5$ ; search up to $t_{\text{max}} = 0.8T$
Smoothing (for $r_E$ )	moving average window $w = 301$ time steps
Ensemble size (main)	$M = 25$ realizations per $(\tau, \text{graph})$
Ensemble size (collapse)	$M = 12$ realizations per $(\tau, \text{graph})$
Uncertainty bars	SEM across realizations; collapse uses $1 - R_r(t_{*,\tau})$ per run

TABLE II: **Graph families.** All graphs are undirected with  $A_{ii} = 0$  and connectivity enforced for ER/WS instances.

Family	Parameters	Instances used
ER	$G(N, p)$	$p \in \{0.04, 0.06, 0.08\}$
WS	$(N, k, \beta)$	$k = 6, \beta = 0.2$
Ring	periodic 1D lattice nearest-neighbor coupling	

recording  $R(t)$  and  $\Psi(t)$  for each realization and reporting ensemble means (and, when relevant, standard deviations).

*e. Operational phase robustness (Option A).* Because the dynamics is  $U(1)$ -invariant,  $\Psi$  is defined only up to an arbitrary global rotation in each realization. To quantify *operational* stability of the emergent reference phase we therefore use a lagged, gauge-fixed variance. For a fixed anchor time  $t_0$  we define the phase lag

$$\Delta\Psi_r(t; t_0) = \text{wrap}(\Psi_r(t) - \Psi_r(t_0)) \in (-\pi, \pi], \quad (32)$$

and the ensemble variance

$$V_\Psi(\Delta t) \equiv \text{Var}_r[\Delta\Psi_r(t_0 + \Delta t; t_0)], \quad \Delta t \geq 0. \quad (33)$$

In the numerics we set  $t_0 = 12$  and estimate  $V_\Psi(\Delta t)$  across realizations. This quantity measures how rapidly the emergent reference phase diffuses over a lag  $\Delta t$  once coherence is present.

*f. Emergence proxy versus  $NR^2$ .* To connect with the scaling discussion of Sec. IV we also plot  $V_\Psi$  as a function of  $NR(t)^2$  along trajectories. For presentation we smooth  $V_\Psi$  with a short moving-average window in time. The resulting curve exhibits the expected suppression of phase fluctuations with increasing  $NR^2$ .

*g. Disagreement energy and tracking ratio.* To robustly probe the spectral tracking/freeze-out mechanism we avoid mode amplitudes that can cross zero and instead use the global disagreement energy

$$E(t) \equiv \|\boldsymbol{\theta}(t) - \bar{\boldsymbol{\theta}}(t)\mathbf{1}\|^2, \quad \bar{\boldsymbol{\theta}}(t) = \frac{1}{N} \sum_{i=1}^N \theta_i(t). \quad (34)$$

From  $E(t)$  we form an energy-based tracking ratio

$$r_E(t) \equiv \frac{-\frac{1}{2} \partial_t \ln E(t)}{K(t)\lambda_2}, \quad (35)$$

where the time derivative is estimated numerically from a smoothed  $\ln E(t)$ . In the linearized regime,  $E(t)$  decays approximately as  $\exp\left(-2 \int^t K(s)\lambda_2 ds\right)$ , so  $r_E(t) \approx 1$  signals adiabatic tracking of the instantaneous relaxation rate, while deviations quantify loss of tracking.

### Operational freeze-out time and prediction

*h. Measured freeze-out time  $t_*$ .* We define an operational freeze-out time  $t_*$  from the trajectory of  $r_E(t)$  using a hysteresis criterion designed to be robust to noise and late-time transients. Specifically, we (i) ignore an initial transient  $t < t_{\text{ignore}} = 0.5$ , (ii) restrict the search to  $t \leq t_{\text{max}}$  with  $t_{\text{max}} = 0.8T$ , and (iii) declare freeze-out when  $r_E(t)$  first drops below a low threshold after having exceeded a high threshold:

$$t_* : \exists t' < t_* \text{ s.t. } r_E(t') > r_{\text{high}}, \quad r_E(t_*) < r_{\text{low}}, \quad r_{\text{high}} = 0.7, \quad r_{\text{low}} = 0.4. \quad (36)$$

For each parameter point we compute  $t_*$  for each realization and report the ensemble mean and standard error.

*i. Predicted freeze-out time.* The spectral balance condition of Sec. V suggests the scale

$$K(t_*)\lambda_2 \sim c \left| \frac{d}{dt} \ln K(t_*) \right| = c \frac{\alpha}{t_* + \tau}, \quad (37)$$

where  $c$  is an order-one constant reflecting the operational definition of tracking loss. We determine  $c$  by calibrating on a single in-window reference point (here  $\tau_{\text{cal}} = 4$  on the main ER graph), and then hold  $c$  fixed when comparing across other  $\tau$  values and across graph families. When (37) has no solution, the parameter point is classified as “no crossing” (always non-adiabatic or always adiabatic by the criterion); when the solution satisfies  $t_* > T$ , it is flagged as “beyond  $T$ ” and not used for quantitative comparison.

## Results

*j. Rate-controlled ordering.* Figure 2 shows  $R(t)$  on the main ER graph ( $N = 80$ ,  $p = 0.06$ ) for several ramp times  $\tau$ . Fast ramps ( $\tau = 0.5$ ) suppress ordering, leading to a significantly lower asymptotic coherence over the simulated time, while slower ramps rapidly generate near-complete coherence ( $R \rightarrow 1$ ) within a few time units. This demonstrates the basic rate-controlled emergence mechanism in a non-spatial setting.

*k. Operational stability of the global phase.* Once coherence has emerged, the global phase becomes highly stable. Figure 3 displays  $V_\Psi(\Delta t)$  for a representative slow ramp ( $\tau = 8$ ) anchored at  $t_0 = 12$ . The variance grows smoothly with lag, consistent with slow phase diffusion of the macroscopic reference phase rather than ill-posedness. Figure 4 shows  $V_\Psi$  against  $NR^2$ , exhibiting strong suppression of phase uncertainty as  $NR^2$  increases, in line with the operational-emergence scaling arguments.

In addition to the  $V_\Psi$  diagnostics shown here, we explicitly operationalize the threshold by defining the emergence time  $t_{\text{em}}(\kappa) = \inf\{t : NR(t)^2 \geq \kappa\}$  and measuring its dependence on protocol parameters. These supplementary diagnostics are reported in Appendix A.

*l. An explicit emergence time from the  $NR^2$  threshold.* To make the  $NR^2$  criterion fully operational, we fix an  $O(1)$  tolerance  $\kappa$  and define the *emergence time* as the first time at which the coherence proxy crosses the threshold,

$$t_{\text{em}}(\kappa) := \inf \left\{ t \geq 0 : NR(t)^2 \geq \kappa \right\}. \quad (38)$$

The interpretation is direct: for  $t < t_{\text{em}}$  the global phase is not reliably estimable, whereas for  $t \geq t_{\text{em}}$  the reference phase becomes stable in the sense of suppressed phase-lag fluctuations. In the numerical experiments of Sec. VII we

use  $\kappa = 8$  (Table I). Consistently with (38), the phase-lag variance  $V_\Psi(\Delta t)$  becomes small once  $NR^2$  exceeds  $\kappa$ : for example, at lags  $\Delta t \sim \mathcal{O}(10)$  we find  $V_\Psi(\Delta t)$  at the level of  $10^{-4}$ – $10^{-3}$  in the high-coherence regime (see Fig. 4), while it is markedly larger when  $NR^2 \lesssim \kappa$ .

The emergence time  $t_{\text{em}}(\kappa)$  extracted from (38) is reported alongside the freeze-out time  $t_*$ , and provides a complementary operational marker for when  $\Psi$  becomes usable.

*m. Tracking ratio and freeze-out.* To connect numerics with the spectral mechanism we examine  $r_E(t)$  defined in (35). A representative trajectory (Fig. 5) illustrates that  $r_E(t)$  remains  $\mathcal{O}(1)$  over an extended interval, validating its role as a tracking diagnostic, while late-time excursions (when  $K(t)$  becomes small and noise dominates) motivate the restricted search window used in the operational definition of  $t_*$ .

*n. Measured versus predicted  $t_*$ .* Figure 6 compares the measured freeze-out time to the prediction from the balance equation (37) with the single calibrated prefactor  $c$ . Across intermediate ramp times where a crossing occurs within the simulated window, the agreement is quantitative within the ensemble uncertainty. For very fast ramps, the balance condition has no solution (system remains non-adiabatic by the criterion), and for very slow ramps the predicted  $t_*$  can exceed  $T$ , in which case no freeze-out is observed within the simulation time.

*o. Spectral collapse across non-spatial graphs and deviation of the ring.* Finally, we test the central organizing variable  $\lambda_2\tau$  across graph families by plotting the residual incoherence at freeze-out,  $1 - R(t_*)$ , versus  $\lambda_2\tau$  on log–log axes. Figure 7 shows that ER and WS graphs approximately collapse onto a common curve spanning several decades in  $1 - R(t_*)$ , supporting the claim that the slowest Laplacian relaxation scale and the protocol timescale jointly control the emergent coherence at freeze-out. Error bars denote the standard error of the mean across realizations (computed from  $1 - R(t_*)$  evaluated per realization at its own measured  $t_*$ ). By contrast, the periodic ring graph systematically deviates from this collapse, remaining far from global coherence even when  $\lambda_2\tau$  is large, consistent with topological-sector trapping and defect-mediated ordering discussed in Sec. VI. This separation cleanly delineates the regime where spectral control suffices (generic networks) from the regime where topological obstructions dominate (periodic spatial graphs).

*p. Reproducibility.* All results in this section are produced by the accompanying Colab implementation, which fixes the random seed, enforces graph connectivity for ER/WS samples, uses  $\mathcal{O}(E)$  coupling evaluation per step, and reports ensemble means and standard errors.

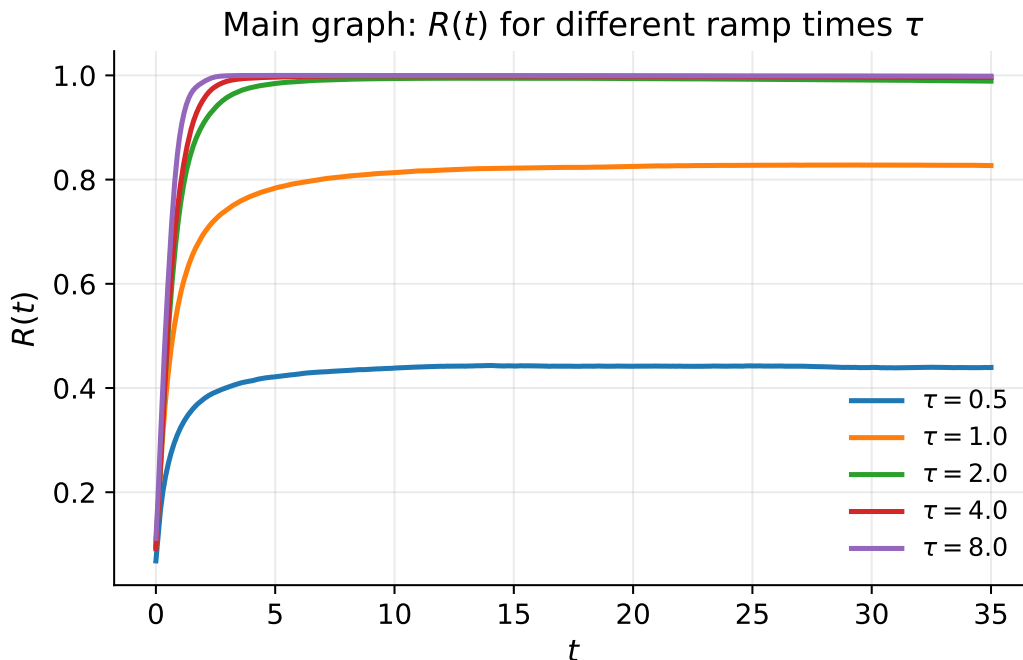


FIG. 2: **Rate-controlled ordering on the main graph.** Time evolution of the Kuramoto order-parameter magnitude  $R(t)$  for several ramp times  $\tau$  under the nonautonomous protocol  $K(t) = K_0(1 + t/\tau)^{-\alpha}$  (parameters as in Sec. VII). Fast ramps suppress coherence, while slower ramps rapidly produce near-complete synchronization.

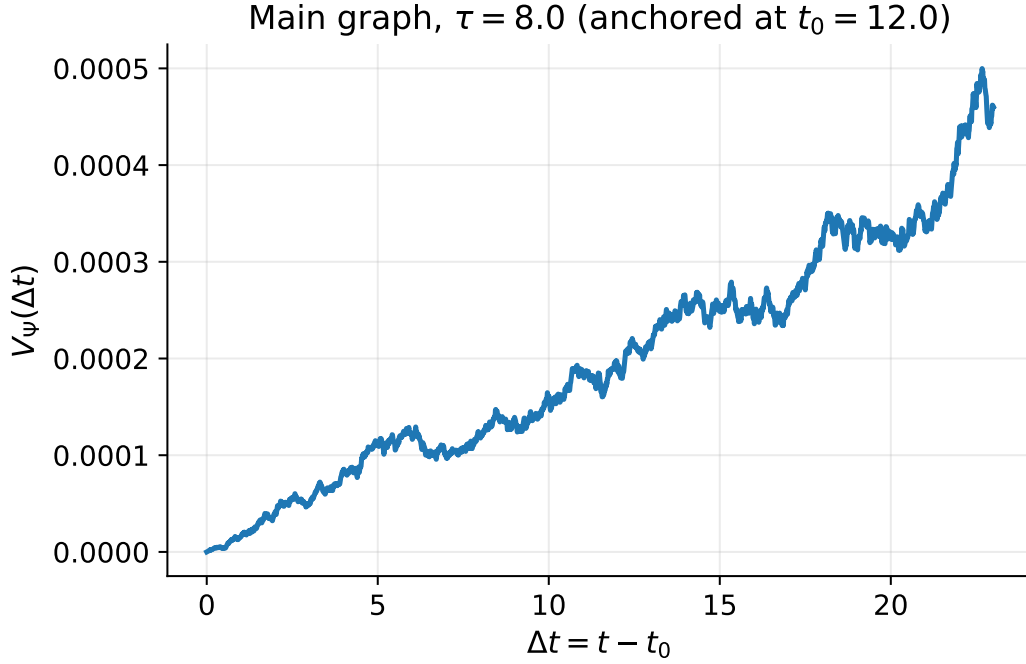


FIG. 3: **Operational stability of the global phase.** Lagged, gauge-fixed phase variance  $V_{\Psi}(\Delta t) = \text{Var}[\text{wrap}(\Psi(t_0 + \Delta t) - \Psi(t_0))]$  for a representative slow ramp, anchored at  $t_0$  (shown in the plot). The smooth growth with  $\Delta t$  indicates slow diffusion of the emergent reference phase once coherence is established.

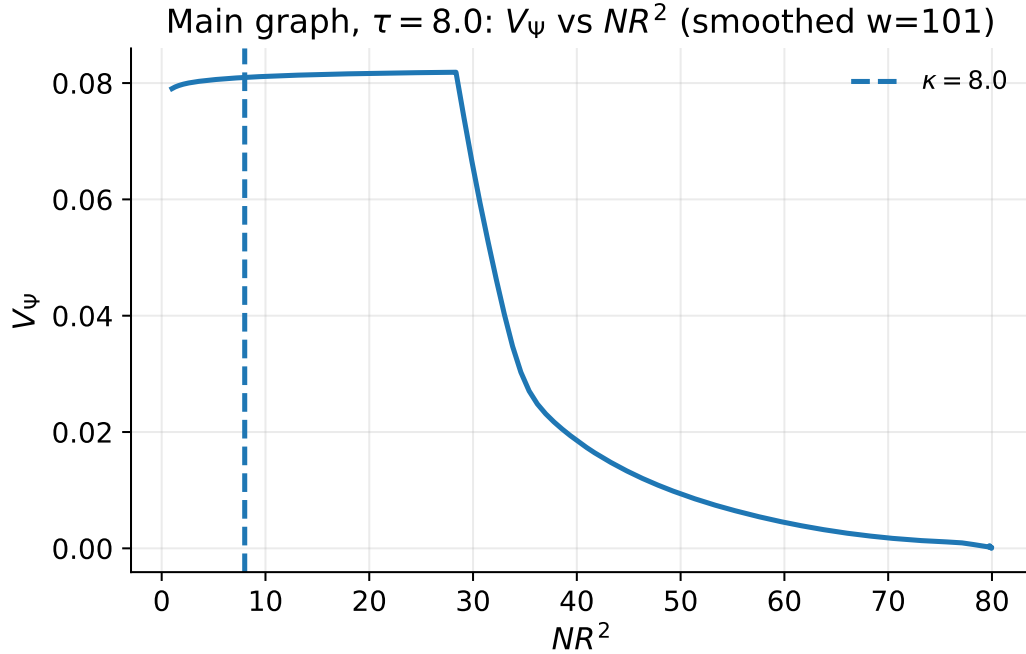


FIG. 4: **Phase robustness versus coherence.** Lagged phase variance  $V_{\Psi}$  plotted against the coherence proxy  $NR^2$  along trajectories (with mild smoothing in time for visualization, as in the code). Phase uncertainty is strongly suppressed as  $NR^2$  increases, supporting the operational-emergence criterion.

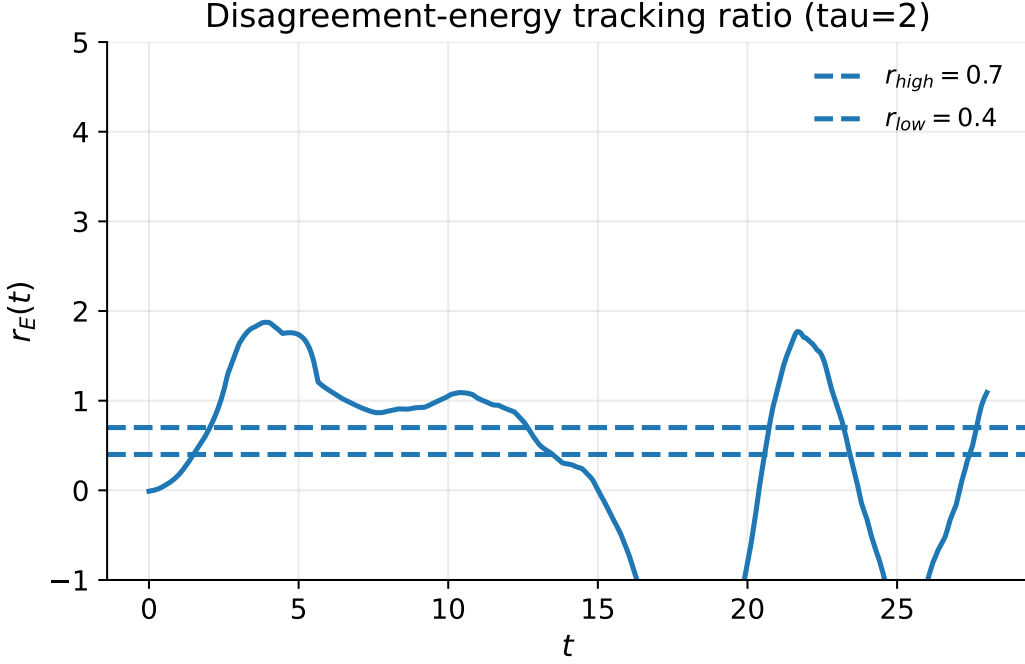


FIG. 5: **Disagreement-energy tracking ratio.** The tracking diagnostic  $r_E(t) = [-\frac{1}{2}\partial_t \ln \|\theta - \bar{\theta}\|^2] / [K(t)\lambda_2]$  for a representative ramp time (here  $\tau = 2$ ), with horizontal reference thresholds  $r_{high}$  and  $r_{low}$ . In the linear tracking regime one expects  $r_E(t) \approx 1$ ; deviations quantify loss of adiabatic tracking and motivate the operational freeze-out definition used to extract  $t_*$ .

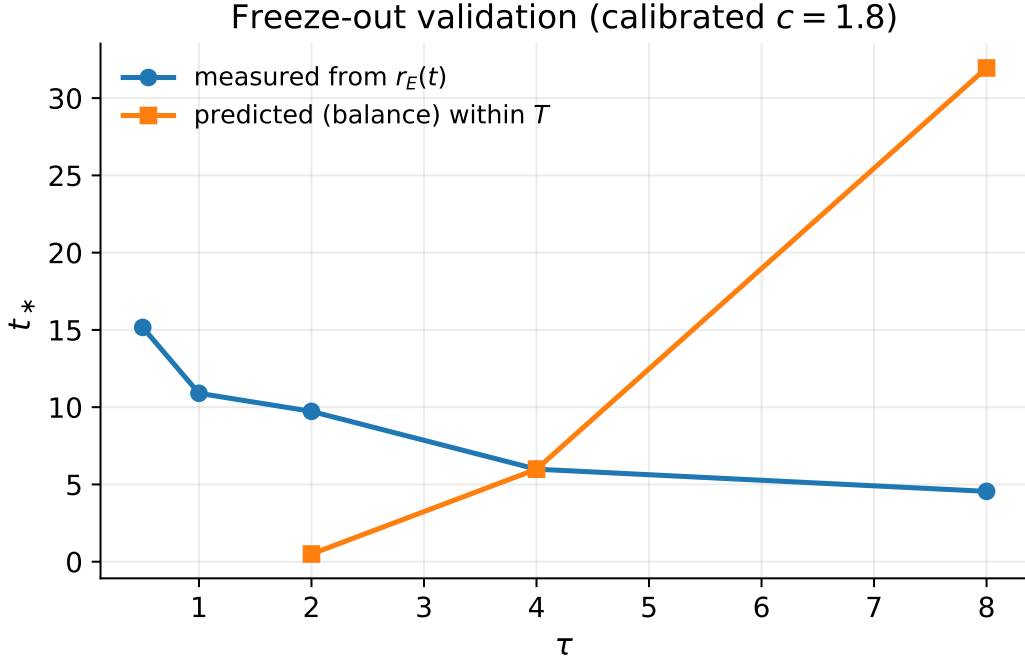


FIG. 6: **Freeze-out time: measured vs. spectral prediction.** Comparison of the measured freeze-out time  $t_*$  (from the energy-ratio hysteresis criterion) with the prediction obtained by solving  $K(t_*)\lambda_2 = c\alpha/(t_* + \tau)$ . The prefactor  $c$  is calibrated on a single in-window reference point and then held fixed. Points with no solution (no-crossing) or with  $t_* > T$  (beyond the simulation window) are treated separately as described in Sec. VII.

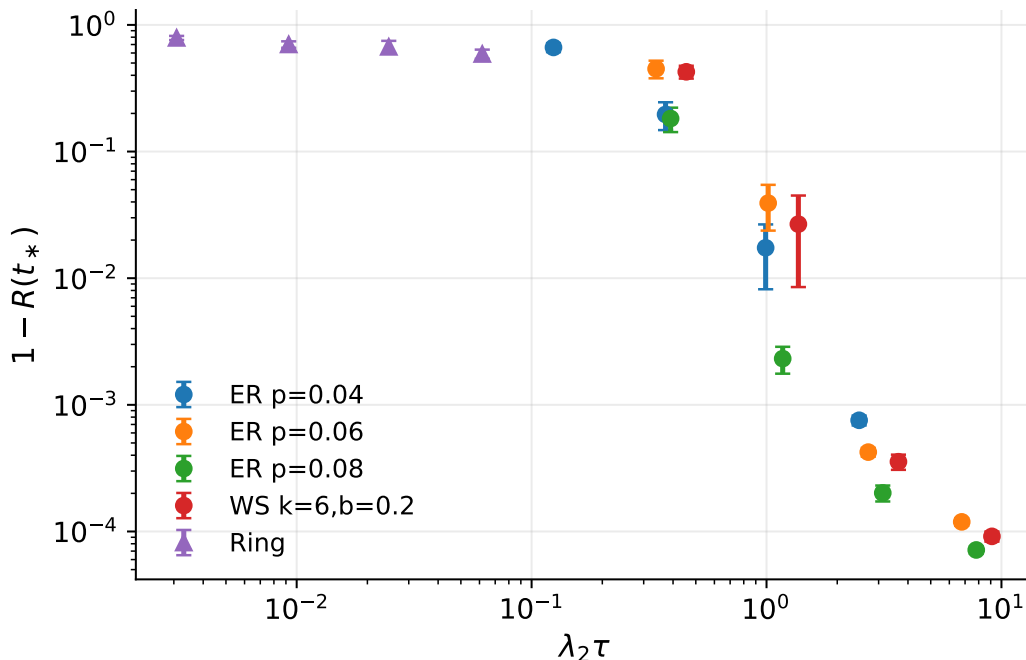


FIG. 7: **Spectral collapse of residual incoherence at freeze-out.** Residual incoherence  $1 - R(t_*)$  (log scale) evaluated at the operational freeze-out time  $t_*$  plotted against the spectral protocol parameter  $\lambda_2 \tau$  (log scale) across graph families. Erdős–Rényi and Watts–Strogatz graphs approximately collapse onto a common curve, while the periodic ring systematically deviates due to topological-sector trapping/defect-mediated ordering. Error bars show the standard error of the mean across realizations, computed from  $1 - R_r(t_{*,r})$  evaluated per realization at its own measured freeze-out time.

## VIII. CONCLUSIONS AND OUTLOOK

We introduced and tested a framework for *nonautonomous synchronization* in which collective order is driven by an explicit coupling protocol  $K(t)$  on a fixed interaction graph. The central conceptual move is to treat the emergence of a global reference phase as an *operational* phenomenon: while the Kuramoto order parameter always defines a formal phase  $\Psi$  whenever  $R > 0$ ,  $\Psi$  becomes meaningful only when it is robust under finite-size fluctuations and weak noise. This motivates a robustness diagnostic based on phase-lag statistics, which turns “global phase” from a definition into a measurable macroscopic coordinate whose utility depends on coherence and system size.

On the dynamical side, we argued that protocol-driven ordering is controlled by a competition between the protocol timescale and the slowest relaxation scale of the graph. In the near-coherent regime, the Laplacian gap  $\lambda_2$  sets the slowest linear decay rate, suggesting a spectral adiabaticity condition and a freeze-out scale defined by a balance between  $K(t)\lambda_2$  and the logarithmic protocol rate  $|\partial_t \ln K|$ . In simulations we validated the organizing role of  $\lambda_2 \tau$  across non-spatial graph families: Erdős–Rényi and small-world networks display an approximate collapse of the residual incoherence  $1 - R(t_*)$  at the operational freeze-out time when plotted against  $\lambda_2 \tau$ , spanning several decades. A key methodological outcome is that the most stable numerical probe of tracking is not a signed mode amplitude, but a positive-definite disagreement energy, which yields a robust tracking ratio and a reproducible operational definition of  $t_*$ .

Periodic spatial graphs behave differently. Rings (and, by extension, higher-dimensional tori) support topological sectors and defects that obstruct global ordering even when spectral conditions suggest rapid relaxation. In this case the dynamics is governed not only by timescale competition but also by sector trapping and defect-mediated coarsening. The resulting systematic deviation from the network collapse cleanly delineates two regimes: (i) generic networks where spectral control captures the dominant protocol dependence, and (ii) periodic spatial topologies where topological constraints provide an additional, genuinely non-mean-field obstruction.

*a. Outlook.* Several directions are immediate and, we expect, broadly transferable beyond the present context.

1. **Beyond scalar coupling protocols:  $A_{ij}(t)$  and multiplex switching.** The present study isolates a clean

nonautonomy source by taking a static graph and a time-dependent coupling amplitude  $K(t)$ . An important extension is to time-varying connectivity (edge switching and rewiring), where protocol nonautonomy enters through  $A_{ij}(t)$  and competes with intrinsic relaxation. Translating the present spectral protocol criterion into switching-network settings should clarify when a time-averaged Laplacian governs tracking and when genuinely non-commuting graph dynamics produces new freeze-out phenomena.

2. **Inertial and driven oscillator models.** Including inertia ( $m > 0$ ) and damping yields the swing equation / inertial Kuramoto class relevant to engineered oscillator networks. Inertia introduces additional timescales and can generate overshoot, oscillatory relaxation, and noise-amplified excursions. A natural question is whether the spectral protocol parameter generalizes from  $\lambda_2$  to a complex relaxation spectrum, and how operational phase emergence is altered when macroscopic oscillations persist.
3. **Topological observables and defect kinetics under protocols.** On periodic lattices, protocol dependence is most naturally expressed in defect statistics (winding, vortex density) rather than solely in  $R(t)$ . A next step is to formulate a protocol-dependent kinetic theory for defect annihilation and sector-changing events, and to connect this explicitly to coarse-grained measures of reference-phase stability. This would provide a principled bridge between spectral timescale competition and Kibble–Zurek-style freeze-out pictures.
4. **A sharper information-theoretic notion of emergent phase.** The lagged phase variance used here is a convenient operational proxy for stability. A more systematic formulation would characterize the estimability of  $\Psi$  via an information metric (e.g. Fisher information for phase inference from finite samples), making explicit the role of noise, sampling, and correlations. This would turn the emergence threshold into a quantitative statistical statement and clarify how “global phase” depends on what is experimentally accessible.
5. **Application-facing reductions.** Although we have emphasized a theoretical and formal development, the model class overlaps with Kuramoto-like reductions used in applications (power-grid synchronization, coupled laser arrays, engineered oscillator networks). The collapse observed in generic networks suggests that protocol design can be parameterized by a small set of spectral quantities, offering a route to low-dimensional control principles: given a target coherence at a deadline, one can constrain admissible protocol families through  $\lambda_2$ -dependent tracking bounds and robustness criteria for the reference phase.

Overall, the nonautonomous viewpoint highlights a simple but powerful idea: synchronization is not only a property of a coupling strength, but of a *history*. By making the emergence of the reference phase operational and linking protocol dependence to graph spectra and topological sectors, this work provides a framework for studying how macroscopic coordination can be created, preserved, or lost under time-dependent interactions.

- 
- [1] V. Sanz, Axion misalignment as a synchronization phenomenon (2026), arXiv:2601.07836 [astro-ph.CO].
  - [2] J. A. Acebrón, L. L. Bonilla, C. J. Pérez Vicente, F. Ritort, and R. Spigler, *Rev. Mod. Phys.* **77**, 137 (2005).
  - [3] F. Dörfler and F. Bullo, *Automatica* **50**, 1539 (2014).
  - [4] J. G. Restrepo, B. R. Hunt, and E. Ott, *Phys. Rev. E* **71**, 036151 (2005), arXiv:cond-mat/0411202.
  - [5] S. Petkoski and A. Stefanovska, *Phys. Rev. E* **86**, 046212 (2012), arXiv:1107.3867.
  - [6] B. Pietras and A. Daffertshofer, *Chaos* **26**, 103101 (2016), arXiv:1608.02723.
  - [7] E. Ott and T. M. Antonsen, *Chaos* **18**, 037113 (2008).
  - [8] M. K. S. Yeung and S. H. Strogatz, *Phys. Rev. Lett.* **82**, 648 (1999).
  - [9] E. Montbrió, D. Pazó, and A. Roxin, *Phys. Rev. E* **74**, 056201 (2006).
  - [10] H. Wu and M. Dhamala, *Phys. Rev. E* **98**, 032221 (2018).
  - [11] S. Chandra, A. Dutta, S. Jana, and D. Ghosh, *Chaos* **31**, 113125 (2021).
  - [12] D. Métivier, I. Tyulkina, B. Sonnenschein, and M. Rosenblum, Bifurcations in the time-delayed Kuramoto model of coupled oscillators (2019), arXiv:1808.10436 (published version available), arXiv:1808.10436.
  - [13] E. Mahdavi and others, *Chaos, Solitons & Fractals* (2026).
  - [14] M. Faggian, M. Franceschet, L. A. Markovich, M. Conti, D. Ronchi, B. Bassetti, and T. Carletti, *Scientific Reports* **9**, 12027 (2019).
  - [15] M. C. Eser and M. Rıza, Interlayer synchronization in time-varying Kuramoto–Sakaguchi networks (2021), arXiv:2111.12753, arXiv:2111.12753.
  - [16] W. Lu and T. Chen, *Networks and Heterogeneous Media* **6**, 329 (2011).
  - [17] R. Leander, P. Hövel, M. Timme, and E. Schöll, *Physica D* **306**, 9 (2015).
  - [18] M. A. Miranda, J. Burguete, V. Pérez-Villar, and H. Mancini, *Phys. Rev. E* **87**, 032902 (2013).
  - [19] Y. Rouzairie and D. Levis, *Frontiers in Physics* **10**, 976515 (2022), arXiv:2206.11730.

- [20] T. E. Lee, E. Ott, and T. M. Antonsen, Vortices and the entrainment transition in the 2D Kuramoto model (2010), arXiv:1006.3600, arXiv:1006.3600.
- [21] M. Sarkar and N. Gupte, Phys. Rev. E **103**, 032204 (2021).
- [22] T. Coletta, R. Delabays, and P. Jacquod, Phys. Rev. E **95**, 042207 (2017), arXiv:1612.07031.
- [23] D. Pazó, Phys. Rev. E **72**, 046211 (2005), arXiv:nlin/0509020.
- [24] O. E. Omel'chenko and G. A. Gottwald, Mean-field approach to finite-size fluctuations in the Kuramoto–Sakaguchi model (2025), arXiv:2511.03700, arXiv:2511.03700.
- [25] A. C. Kalloniatis, M. L. Zuparic, and M. Prokopenko, Phys. Rev. E **98**, 022302 (2018).
- [26] P. Ashwin, S. Wicczorek, R. Vitolo, and P. Cox, Chaos **28**, 033501 (2018).
- [27] H. Alkhayuon, P. Ashwin, and S. Wicczorek, Proceedings of the Royal Society A **477**, 20210059 (2021).
- [28] G. Filatrella, A. H. Nielsen, and N. F. Pedersen, Eur. Phys. J. B **61**, 485 (2008), arXiv:0705.1305.

### Appendix A: Estimability scaling for the collective phase

This appendix makes precise in what sense the collective phase  $\Psi$  is an *operational* macroscopic coordinate. The key point is that, even though  $\Psi = \arg Z$  is formally defined whenever  $R > 0$ , it is statistically meaningful only when it is *estimable* with small uncertainty from finite noisy samples. In the coherent regime we show (at the scaling level) that phase uncertainty is suppressed as  $1/(NR^2)$ , motivating an explicit threshold  $NR^2 \gtrsim \kappa$  and an associated *emergence time*  $t_{\text{em}}(\kappa)$ . We then connect this operational definition to the numerical diagnostics and the spectral organization observed in the main text.

*a. Setup.* Let

$$Z = \frac{1}{N} \sum_{j=1}^N e^{i\theta_j} = Re^{i\Psi}. \quad (\text{A1})$$

In a coherent regime, phases cluster around a mean direction  $\Psi$  with small fluctuations. Write  $\theta_j = \Psi + \delta_j$  with  $\langle \delta_j \rangle = 0$  and  $|\delta_j| \ll 1$ . To leading order,

$$e^{i\theta_j} = e^{i\Psi} \left( 1 + i\delta_j - \frac{1}{2}\delta_j^2 + \dots \right), \quad Z = e^{i\Psi} \left[ 1 + \frac{i}{N} \sum_j \delta_j - \frac{1}{2N} \sum_j \delta_j^2 + \dots \right]. \quad (\text{A2})$$

Hence  $\text{Im}(e^{-i\Psi} Z) \simeq \frac{1}{N} \sum_j \delta_j$ , while  $R \simeq 1 - \frac{1}{2N} \sum_j \delta_j^2$  encodes the fluctuation level.

*b. Delta-method estimate for the phase variance.* For small noise, the estimator  $\widehat{\Psi} = \arg Z$  admits the first-order approximation

$$\widehat{\Psi} - \Psi \simeq \frac{\text{Im}(e^{-i\Psi} \delta Z)}{|Z|} \simeq \frac{1}{R} \frac{1}{N} \sum_{j=1}^N \delta_j, \quad (\text{A3})$$

where  $\delta Z$  denotes fluctuations of  $Z$  around its mean. If the  $\delta_j$  have variance  $\sigma^2$  and are weakly correlated so that  $\text{Var}\left(\frac{1}{N} \sum_j \delta_j\right) \sim \sigma^2/N$ , then

$$\text{Var}(\widehat{\Psi}) \sim \frac{\sigma^2}{NR^2}. \quad (\text{A4})$$

In stochastic phase dynamics with weak independent noise one expects  $\sigma^2 \propto D_{\text{eff}}$ , where  $D_{\text{eff}}$  collects model-dependent prefactors (observation noise, filtering, residual correlations), yielding

$$\text{Var}(\widehat{\Psi}) \sim \frac{D_{\text{eff}}}{NR^2}. \quad (\text{A5})$$

Equation (A5) makes the operational point explicit: as  $R \rightarrow 0$  the phase becomes ill-posed (order-one uncertainty), while increasing  $NR^2$  suppresses fluctuations.

*c. Connection to Fisher information (CRLB).* The scaling (A5) is consistent with an information bound: in models where  $\Psi$  enters as a mean-direction parameter, the Fisher information scales as  $\mathcal{I}_{\Psi} \propto NR^2/D_{\text{eff}}$ , hence the Cramér–Rao bound gives  $\text{Var}(\widehat{\Psi}) \gtrsim D_{\text{eff}}/(NR^2)$ . Correlations renormalize  $D_{\text{eff}}$  but preserve the  $1/(NR^2)$  suppression in the coherent regime.

*d. Operational threshold and emergence time.* Fixing a tolerance  $\kappa = O(1)$ , we define an operational emergence condition by requiring  $NR^2 \gtrsim \kappa$ . This motivates the *emergence time*

$$t_{\text{em}}(\kappa) = \inf\{t : NR(t)^2 \geq \kappa\}, \quad (\text{A6})$$

used in the numerical analysis. Figure 8 illustrates  $t_{\text{em}}$  versus the protocol timescale  $\tau$  on the main network instance (parameters as in Table I), demonstrating that slower protocols bring the system into the estimable regime earlier and with reduced run-to-run variability.

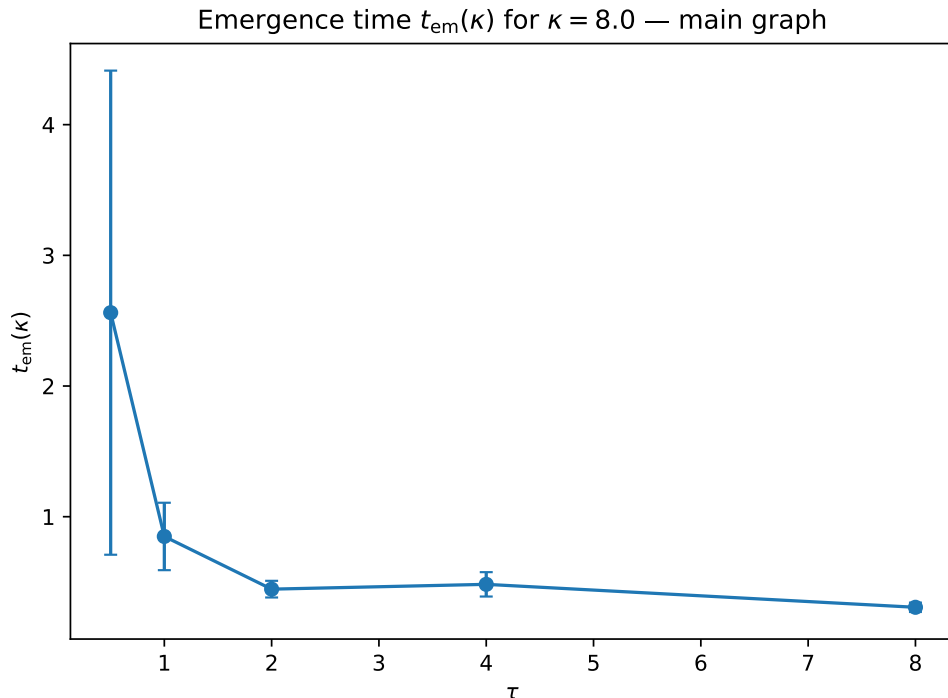
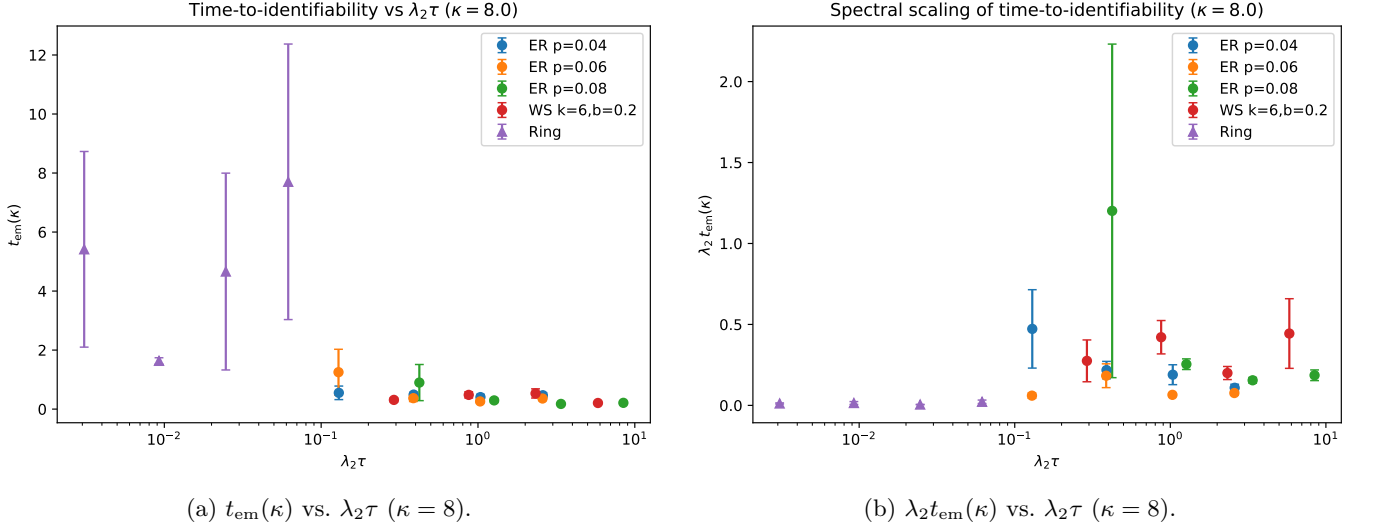


FIG. 8: **Emergence time versus protocol timescale.** Emergence time  $t_{\text{em}}(\kappa) = \inf\{t : NR(t)^2 \geq \kappa\}$  as a function of the ramp time  $\tau$  for  $\kappa = 8$ . Points show ensemble means over realizations and error bars denote the SEM.

*e. Spectral organization of time-to-identifiability.* The central message of the main text is that protocol dependence on generic networks is organized by a competition between the protocol timescale and graph relaxation, controlled by the Laplacian gap  $\lambda_2$ . To test whether the *entry* into the estimable regime is similarly organized, we plot  $t_{\text{em}}(\kappa)$  against the spectral protocol parameter  $\lambda_2\tau$  across graph families. As shown in Fig. 9, non-spatial networks (Erdős–Rényi and Watts–Strogatz) exhibit a systematic decrease of  $t_{\text{em}}$  with  $\lambda_2\tau$ , and an improved collapse when plotted in the dimensionless form  $\lambda_2 t_{\text{em}}$ . This supports the interpretation that  $\lambda_2^{-1}$  sets the dominant relaxation scale controlling the time-to-identifiability under nonautonomous coupling protocols. Periodic rings deviate systematically, consistent with the additional constraint of topological-sector trapping/defect-mediated dynamics.

(a)  $t_{em}(\kappa)$  vs.  $\lambda_2 \tau$  ( $\kappa = 8$ ).(b)  $\lambda_2 t_{em}(\kappa)$  vs.  $\lambda_2 \tau$  ( $\kappa = 8$ ).

**FIG. 9: Spectral organization of the time-to-identifiability.** For each graph instance and ramp time  $\tau$ , we compute the emergence time  $t_{em}(\kappa) = \inf\{t : NR(t)^2 \geq \kappa\}$  with  $\kappa = 8$ ; points show ensemble means and error bars show SEM. Non-spatial networks exhibit substantial organization by  $\lambda_2 \tau$ , and improved collapse in the dimensionless combination  $\lambda_2 t_{em}$ , consistent with  $\lambda_2^{-1}$  controlling relaxation. Rings deviate due to topological obstruction; moreover  $\lambda_2 \sim N^{-2}$  on rings is parametrically small, so  $\lambda_2 t_{em}$  can be small even when  $t_{em}$  is large, highlighting that topology introduces a distinct slow mechanism beyond spectral relaxation.